Available online at www.sciencedirect.com
ScienceDirect
Journal of Molecular Catalysis A: Chemical 269 (2007) 149–157
JOURNAL OF MOLECULAR CATALYSIS A: CHEMICAL
www.elsevier.com/locate/molcata

Preparation and characterization of amorphous Co-B catalysts with mesoporous structure

Tong Dong-ge [a,*], Chu Wei [a,*], Luo Yong-yue [b], Chen Hong [c], Ji Xiao-yang [c]

[a] *Lab 230, College of Chemical Engineering, Sichuan University, Chengdu 610065, China*
[b] *State Key Laboratory of Polymer Materials, Sichuan University, Chengdu 610065, China*
[c] *Analytic and Testing Center, Sichuan University, Chengdu 610064, China*

Received 15 December 2006; received in revised form 8 January 2007; accepted 9 January 2007
Available online 16 January 2007

Abstract

Amorphous Co-B alloy catalyst with mesoporous structure was firstly prepared via reduction of cobalt acetate by potassium borohydride in the presence of an organic template hexadecyl–trimethyl–ammonium bromide. The as-prepared mesoporous Co-B was characterized by Fourier transform infrared (FTIR), X-ray powder diffraction (XRD), scanning electron micrograph (SEM), inductively coupled plasma (ICP), X-ray photoelectron spectroscopy (XPS), cyclic voltammetry (CV) measurement, N_2 adsorption–desorption, CO temperature-programmed desorption (TPD), and magnetic performance test. Investigations demonstrated that such mesoporous structure has a pronounced influence on the magnetic properties of Co-B alloy and the enhanced magnetic performance enables the as-prepared mesoporous Co-B to be recycled by magnetic method in the liquid-phase cinnamaldehyde (CMA) hydrogenation. During the hydrogenation, the as-prepared mesoporous Co-B exhibited higher cinnamaldehyde conversion and cinnamyl alcohol (CMO) selectivity than the regular Co-B obtained without using organic template, which is attributed to the larger specific surface area and the stronger affinity to C=O. After 11 cycles, the conversion of cinnamaldehyde over the mesoporous Co-B was 85.2%, which is higher than that of the fresh regular Co-B. The good cycle performance is attributed to its preserved mesoporous structure in spite of the collapse of some mesopores during cycling. In addition, the increase of selectivity for cinnamyl alcohol after several cycles is attributed to the growth of particle size.

Keywords: Mesoporous Co-B; Cinnamaldehyde; Hydrogenation; Cycle performance; Magnetic properties

1. Introduction

Over the past few years, Co-B amorphous alloy, which is nonporous, has been reported as a powerful catalyst in selective hydrogenation of α,β-unsaturated carbonyl compounds to alcohols due to its higher activity and better selectivity [1–3]. The majority of published research has concentrated on the effect of different supports, crystallinity, and the addition of second metals on the selectivity of the catalysts for selective hydrogenation [1–3]. It is well known that the catalytic properties of metal catalysts are in some extent affected by their specific surface areas [4]. Recently, mesoporous metals with high specific surface areas, which are prepared via organic template method, have caused much attention due to their promising application in catalysts [5–7]. However, to our best knowledge, there are few reports for the study of mesoporous Co-B amorphous alloy catalyst.

In this work, amorphous Co-B with mesoporous structure was firstly prepared via reduction of cobalt acetate by potassium borohydride in the presence of an organic template hexadecyl–trimethyl–ammonium bromide and examined as catalysts for liquid-phase cinnamaldehyde (CMA) hydrogenation. The catalytic properties were compared with the regular Co-B obtained without using organic template. The influence of mesoporous structure on the magnetic properties of Co-B alloy was studied in order to recycle the as-prepared mesoporous Co-B catalyst by a simple, economic magnetic method.

* Corresponding authors. Tel.: +86 28 8540 0591/3836; fax: +86 28 8540 3397.
E-mail addresses: tongdongge@163.com (D.-g. Tong), chuwei65@yahoo.com.cn (W. Chu).

1381-1169/$ – see front matter © 2007 Elsevier B.V. All rights reserved.
doi:10.1016/j.molcata.2007.01.016

2. Experimental

2.1. Catalyst preparation

The mesoporous Co-B particles were prepared as follows. All the reagents were of analytical grade. Twenty milliliters hexadecyl–trimethyl–ammonium bromide (CTAB) (0.32 mol/L) aqueous solution was added to a 20 mL cobalt acetate (0.5 mol/L) solution at 318 K and was well mixed by stirring (200 rpm) for 45 min. After 8 h of aging, 20 mL of 2 mol/L potassium borohydride aqueous solution containing 0.2 mol/L NaOH was added dropwise (2.5 mL/min) under stirring (200 rpm) at ice-bath. When no bubbles were released, the black precipitate was washed with distilled water three times, followed by ethanol three times. Then the sample was transferred into 1000 mL of absolute alcohol, and the resulted mixture was refluxed at 353 K for 16 h. The as-prepared material was collected and washed with ethanol five times and finally kept in absolute ethanol until use.

The regular Co-B was prepared by the same method for the mesoporous Co-B but without adding the organic template CTAB.

2.2. Characterization

The FTIR spectra of the samples were measured using the KBr wafer technique in a Nicolet 510SX FTIR spectrometer. The spectra were recorded in the range of 400–4000 cm^{-1}. X-ray diffraction (XRD) patterns of the samples were acquired on D/rmax-rA X-ray diffractometer with Cu Kα sources. During the characterization, the ethanol wet Co-B sample was used and dried in situ in the atmosphere of Ar (Purity of 99.99%, treated with a Chrompack clean-oxygen filter) to protect the sample from oxidation. The compositions of the samples were analyzed by inductively coupled plasma (ICP, Irris, Avantage). The surface morphologies were observed by means of a scanning electron microscopy (SEM, JEOL JSM-6500FE). X-ray photoelectron spectroscopy (XPS) was performed on a Perkin-Elmer 5000C ESCA system using Al Kα radiation to determine the surface electronic states of Co-B particles. Similarly, the Co-B samples were also dried in situ in pure Ar atmosphere to avoid oxidation. All the binding energy values were calibrated by using C1s = 284.6 eV as a reference. The surface composition was determined by using 0.13 and 2.50 as the sensitivity factors to B1s and $Co2p_{3/2}$, respectively, offered by Perkin-Elmer Company [8]. The cyclic voltammetry measurement was performed in a three-electrode cell using a small piece (9 mm^2) of the mesoporous Co-B electrode as working electrode, a large area air electrode as counter electrode, and Hg/HgO in 30% KOH solution as reference electrode. The mesoporous Co-B electrode prepared firstly by mixing 85% mesoporous Co-B particles, 7% polytetrafluoroethylene (PTFE) and 8% carbon black into paste, then roll-pressing the paste to 0.15 mm thick films, and finally pressing film onto a nickel mesh. The air electrode was prepared according to the preparation procedures described in [9]. The specific surface area, total pore volume, and average pore diameter were measured by the nitrogen absorption at 77 K after degassing at 573 K for 3 h. The surface area was calculated by using the conventional Brunauer–Emett–Teller (BET) method. The reproducibility was checked by repeating runs at least three times and was found to be within acceptable limits (±1%). The total pore volume was calculated from the amount of vapor absorbed at a relative pressure (P/P_0) close to unity. Pore size distributions were obtained by using the Barrett–Joyner–Halenda (BJH) model and the desorption branch. The room temperature magnetic characterization of the sample was performed by a vibrating sample magnetometer (MagLab-12, Oxford). CO temperature-programmed desorption (TPD) was performed in the following procedure. Firstly, the air on the sample surface was removed with a nitrogen steam (purity of 99.99%, treated with a Chrompack clean-oxygen filter) at 573 K for 1 h and the surface was cooled to room temperature in the same nitrogen steam. Then, CO was pre-adsorbed by the catalyst at 383 K for 2 h. The CO steam was then replaced with the carrier gas, which was kept at 383 K for 2 h in order to purge the gaseous and physical-absorbed CO away from the catalyst surface. After the surface was cooled down to room temperature, the CO desorption was carried out by raising the temperature at a speed of 40 K/min up to 573 K, then the released CO was determined by an on-line gas chromatograph (GC) equipped with thermal conductivity detector (TCD).

2.3. Activity test

Hydrogenation of CMA was carried out in a 100 mL stainless autoclave equipped with a magnetic stirrer and an electric heating system. After addition of 4.5 mL CMA, 40.5 mL absolute ethanol, and 0.25 g catalysts, the reactor was sealed and washed with H_2 more than four times to exclude air. Then it was filled with H_2 up to 4.2 MPa, followed by heating until 353 K. Once the pressure reached a steady state, the hydrogenation reaction was initiated immediately by stirring the reaction mixture vigorously (1100 rpm). The initial rate of reaction was obtained by measuring the drop of H_2 within the first 0.5 h, from which the specific activity was calculated by using the ideal gas equation. Reaction products were analyzed on SC-200 with flame ionization detection (FID) by means of SE-30 column at 525 K with flowing N_2 as carrier gas.

3. Results and discussion

3.1. FITR spectra

Fig. 1 shows the FTIR spectra of mesoporous Co-B before and after ethanol extraction, and regular Co-B, respectively. Compared with Fig. 1a–c, one can see that after ethanol extraction, the absorbance peaks at 3000–2800, 1500–1400, 962, 912 and 725 cm^{-1} corresponding to the stretching vibration of C–H, the deformation vibration of C–H, the stretching vibration of C–C, the stretching vibration of N–H, and the rocking vibration of C–H in the organic template CTAB molecule, respectively [10], disappeared and the as-prepared mesoporous Co-B shows almost the same FTIR spectrum as the regular Co-B. The results indicated that the applied CTAB organic template

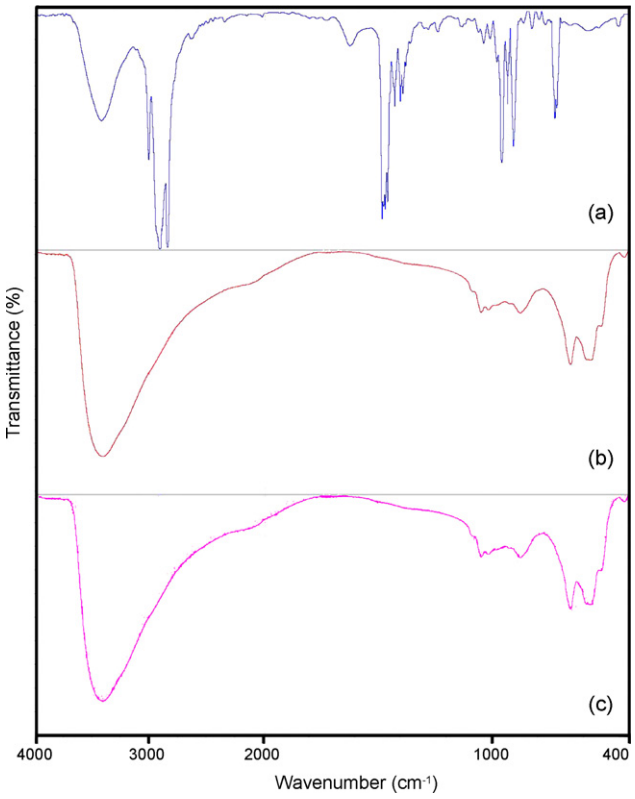

Fig. 1. FTIR spectra of (a) mesoporous Co-B before ethanol extraction; (b) mesoporous Co-B after ethanol extraction; (c) regular Co-B.

had been successively removed by ethanol extraction from the as-prepared Co-B, and the formed mesoporous structure did not affect the vibration behavior of Co-B significantly. The absorbance peaks at 400–600 cm^{-1} in the as-prepared mesoporous Co-B and the regular Co-B (Fig. 1b and c) are attributed to the vibration of Co-B alloy [11].

3.2. Analysis of mesoporous structure

Fig. 2 presents the XRD patterns of the as-prepared mesoporous Co-B. As shown in Fig. 2, only one broad peak around $2\theta = 45.5°$ is observed. It indicates that the as-prepared Co-B has a typical amorphous alloy structure [1–3]. The small-angle XRD pattern of the prepared Co-B, as shown in the inset of Fig. 2, displays a well-resolved diffraction peak around of $2\theta = 1.52°$, implying the presence of mesoporous structure in the as-prepared Co-B [12]. The bulk composition of the as-prepared mesoporous Co-B is shown in Table 1.From Table 1, it can be seen that the bulk composition is almost the same as that of the regular Co-B.

The formed mesoporous structure is also confirmed by N_2 adsorption–desorption isotherm (Fig. 3). The isotherm shows a typical IUPAC type IV pattern with inflection of N_2 adsorbed at P/P_0 about 0.40 (type H4 hysteresis loop) [12], indicating the presence of mesopores. The pore size distribution of the sample, as presented in the inset of Fig. 3, shows that the as-prepared mesoporous Co-B with a narrow pore size distribution has an average pore diameter about 7 nm.

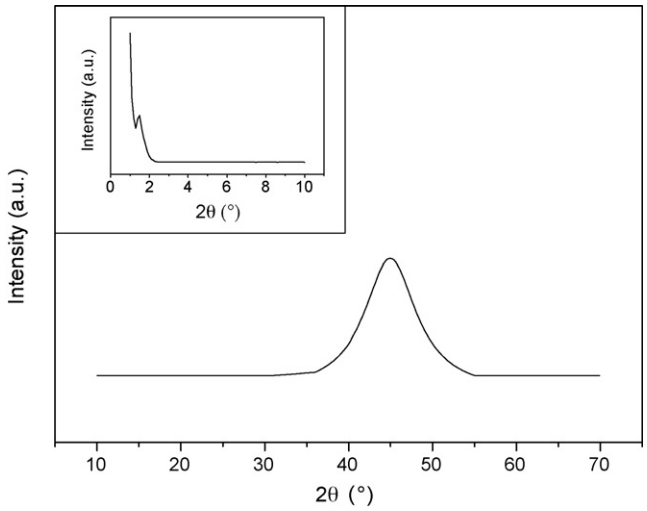

Fig. 2. XRD pattern of the as-prepared mesoporous Co-B. The inset is the small-angle XRD pattern of the as-prepared mesoporous Co-B.

Table 1 presents the specific surface areas of the as-prepared mesoporous Co-B and the regular Co-B. From Table 1, one can see that the specific surface area of the as-prepared mesoporous Co-B (176.27 m^2/g) is much larger than that of the regular Co-B (65.00 m^2/g), which is due to the formation of the mesoporous structure in the as-prepared mesoporous Co-B.

3.3. Surface morphology and formation mechanism of mesoporous structure

Fig. 4a and b show the low and high magnification SEM images of the as-prepared mesoporous Co-B, respectively. A worm-like porous structure can be observed. The pore size distribution is in the mesoporous range, which further confirmed the formation of mesoporous structure in the as-prepared mesoporous Co-B [12].

According to the proposed scheme for synthesis of MCM-41 with mesoporous structure using the organic template CTAB

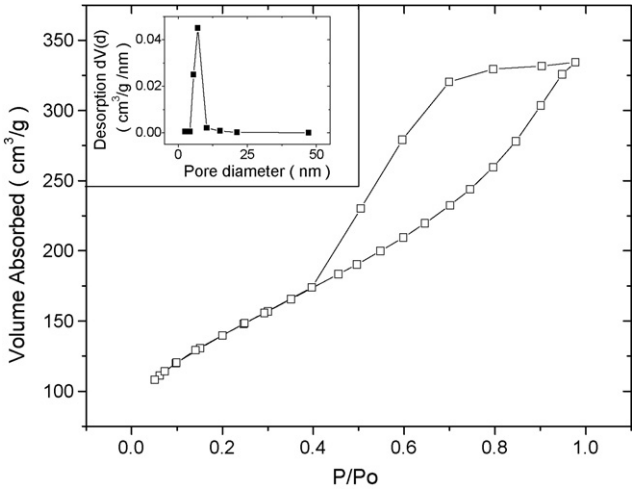

Fig. 3. Nitrogen adsorption–desorption isotherm patterns and the pore size distribution (inset) of the as-prepared mesoporous Co-B.

Table 1
Physicochemical properties and catalytic properties of fresh and spent Co-B particles

Sample		Bulk composition (at.%)	Surface composition (at.%)	Specific surface area (m^2/g)	Pore diameter (nm)	Pore volume (cm^3/g)	R^m (mmol/(h g Co))
Regular Co-B	Fresh	$Co_{63.0}B_{37.0}$	$Co_{58.4}B_{41.6}$	65.00	–	–	215.77
Mesoporous Co-B	Fresh	$Co_{63.0}B_{37.0}$	$Co_{56.7}B_{43.3}$	176.27	7.10	0.43	891.93
	6 cycles	$Co_{63.0}B_{37.0}$	$Co_{56.7}B_{43.3}$	125.34	6.12	0.26	495.40
	11 cycles	$Co_{63.0}B_{37.0}$	$Co_{56.7}B_{43.3}$	93.69	3.66	0.14	334.47

Reaction conditions: 0.25 g catalyst, 4.5 mL CMA, 40.5 mL ethanol at $PH_2 = 4.2$ MPa and $T = 353$ K.

[12], the formation of mesoporous Co-B might be described in Fig. 5. Firstly, Co^{2+} and CTAB assemble together. Then the nanocomposites containing ordered surfactant lyotropic liquid crystalline phase with a micellar structure are formed. Secondly, the assembled Co^{2+} in the formed nanocomposites is reduced by KBH_4. As a result, the formed Co-B surrounds the micellar structure, which is combined into a Co-B cluster as a wall of the mesopore through metallic bonding and/or –Co-B–Co-B– bonding [12]. Many clusters closely pack to form secondary Co-B particles. Finally, the ethanol extraction of organic template CTAB results in the formation of mesoporous structure for Co-B particles.

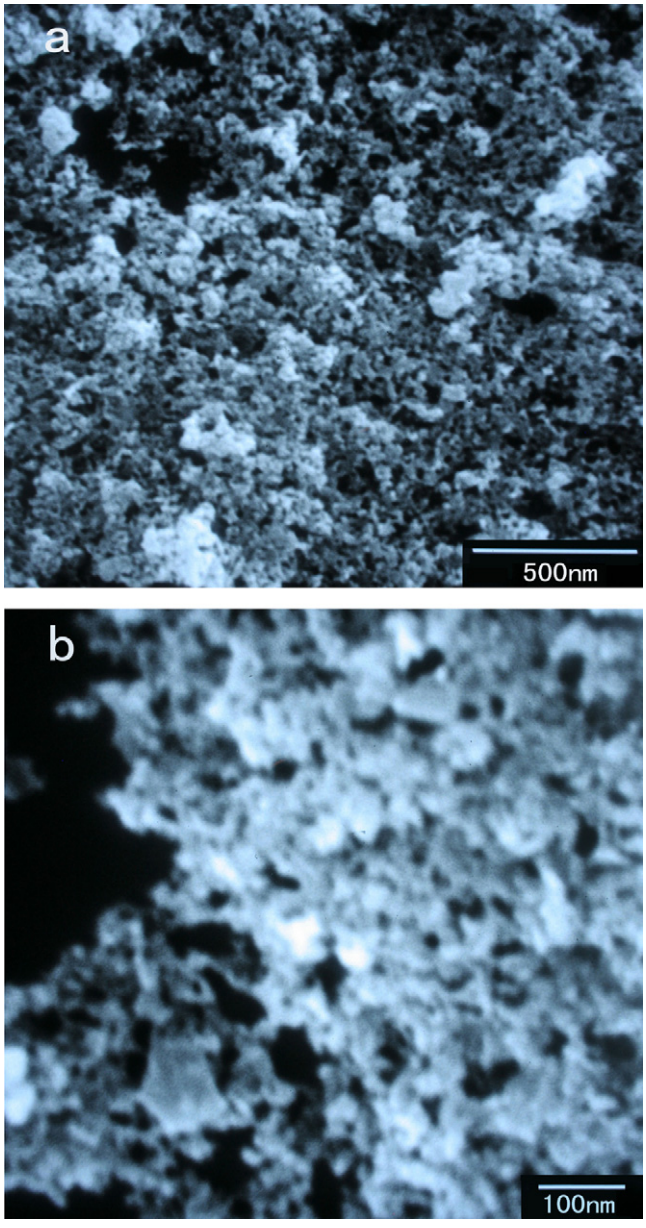

Fig. 4. SEM images of the as-prepared mesoporous Co-B (a) ×30,000 and (b) ×100,000 magnified.

3.4. XPS analysis and cyclic voltammetry measurements

Fig. 6a and b present the $Co2p_{3/2}$ and B1s spectra of the as-prepared mesoporous Co-B particles, respectively. The surface composition is listed in Table 1.

As shown in Fig. 6a, the Co species in the Co-B sample are present in the metallic state with the binding energy 778.1 eV, which is almost the same as that reported [1–3]. Meanwhile, the B species are present in the elemental state with a binding energy of 188.4 eV (Fig. 6b), which is positively shifted 1.3 eV in comparison with the pure B (187.1 eV) [8]. The result indicates the existence of synergistic effect between the Co and B in the as-prepared mesoporous Co-B, as those reported in regular Co-B amorphous alloy [1–3].

The formation of an alloy between Co and B is also confirmed by the electrochemical activation of the mesoporous Co-B when it was used as the anodic material in aqueous alkaline solution. Fig. 7 shows the cyclic voltammogram of mesoporous Co-B in 30% KOH solution. In parallel experiments, pure Co, pure B, and the mixture of pure Co and B did not give any appreciable current response in the sweeping potential region, because they are completely electrochemical inert in aqueous alkaline solution [13,14]. However, in the case of mesoporous Co-B, a large anodic current peak appeared with the onset of oxidation at −0.90 V (Fig. 7), suggesting the electrochemical activation of mesoporous Co-B. It is attributed to that the synergistic effect between Co and B in the Co-B alloy weakened the chemical stability of B and enhanced the chemical activity of Co [15,16].

Furthermore, as shown in Table 1, one can see that the formation of mesoporous structure causes the enrichment of B on the Co-B alloy surface. But the origin for this phenomenon is not fully understood now and is subject further investigations.

3.5. Magnetic properties

Amorphous Co-B catalyst can be recycled by magnetic method [3]. In order to collect the as-prepared mesoporous Co-B

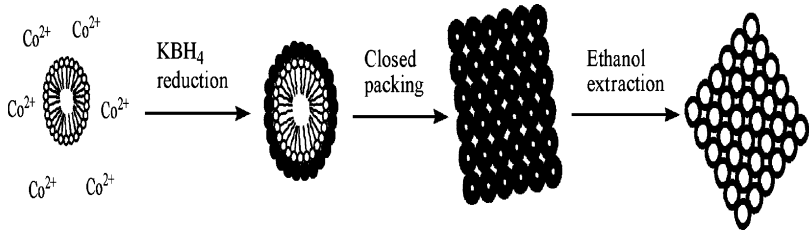

Fig. 5. A possible mechanism for the formation of the as-prepared mesoporous Co-B.

catalysts by magnetic method for reuse, the influence of mesoporous structure on the magnetic properties of Co-B had been investigated. Fig. 8a and b show the hysteresis loop of the regular and mesoporous Co-B at 300 K, respectively. The corresponding coercivity (H_c), saturation magnetization (M_s), and remanet magnetization (M_r) at 300 K are also presented in Fig. 8a and b, respectively.

Compared with M_s (45.7 emu/g) and M_r (16.5 emu/g) of the regular Co-B, M_s and M_r of the as-prepared mesoporous Co-B have comparable values, indicating that the mesoporous structure has little effect on M_s and M_r. However, the H_c of the mesoporous Co-B is much higher than that of the corresponding regular Co-B, indicating that the mesoporous structure has a pronouncing influence on the magnetic properties. The improved magnetic properties for the as-prepared mesoporous Co-B enable it more easily to be collected by magnetic method for reuse.

3.6. Catalytic performance

Under the experimental conditions in this work, the evaluation for external and internal diffusion in the CMA hydrogenation reaction over the regular and mesoporous Co-B (not shown here) according to the method provided by Guo [17] indicated that the effect of external and internal diffusion was negligible. In other words, the mass transfer was significantly eliminated and the CMA hydrogenation was controlled by the intrinsic kinetics of the reaction.

3.6.1. Hydrogenation profile

The catalytic performance of the as-prepared mesoporous Co-B was examined and compared with regular Co-B during liquid-phase CMA hydrogenation. The selective hydrogenation of CMA is a well-documented reaction, which could be represented by the scheme in Fig. 9.

Fig. 10 is the CMA hydrogenation profile over the regular and as-prepared mesoporous Co-B. Table 1 shows the specific activity presented by H_2 uptake rates per gram of cobalt (R^m) of both Co-B catalysts.

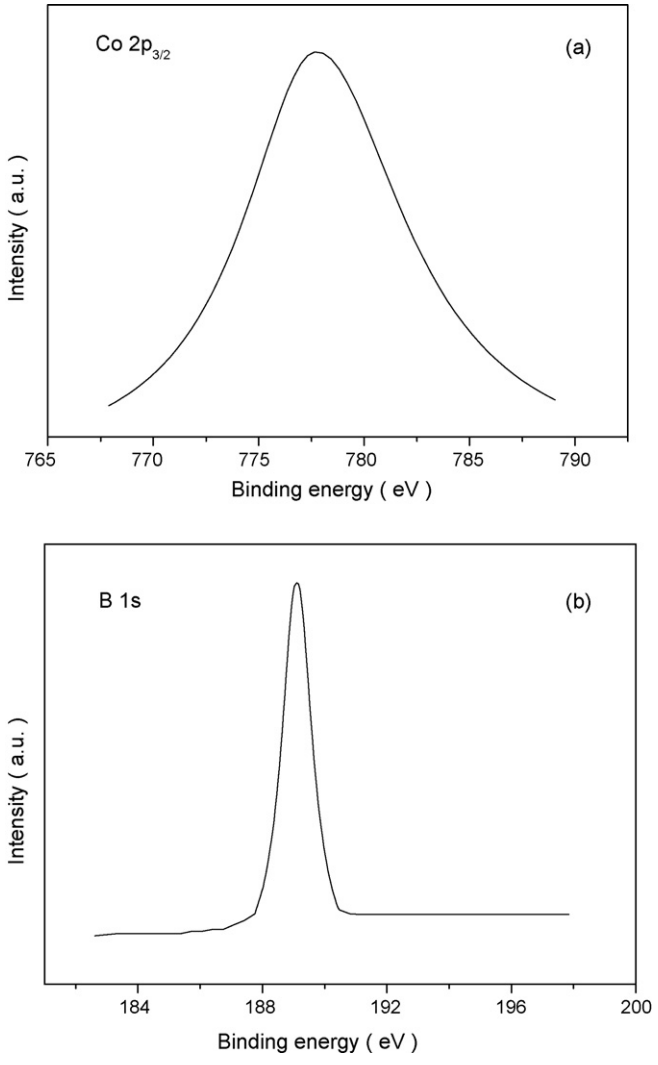

Fig. 6. XPS spectra of the as-prepared mesoporous Co-B (a) Co2p$_{3/2}$; (b) B1s.

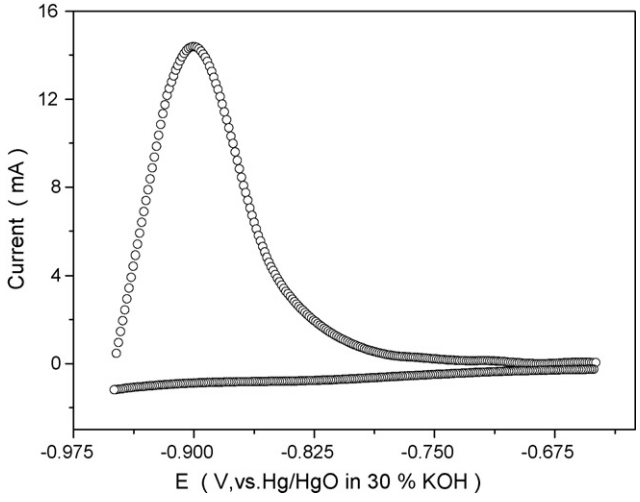

Fig. 7. Cyclic voltammogram of the as-papered mesoporous Co-B in a 30% KOH solution at a potential sweep rate of 0.013 mV/s.

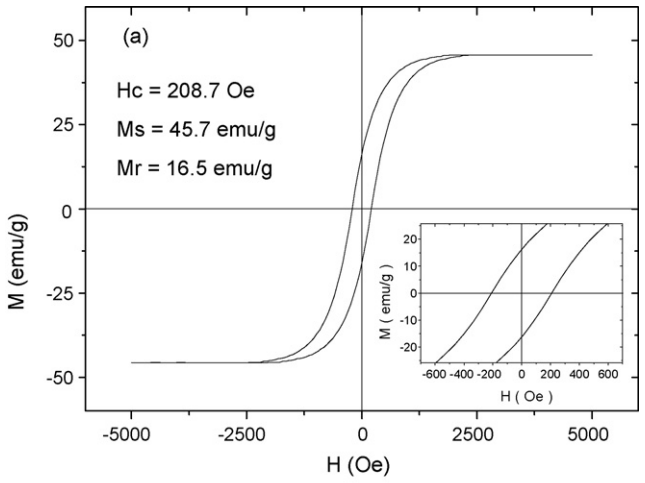

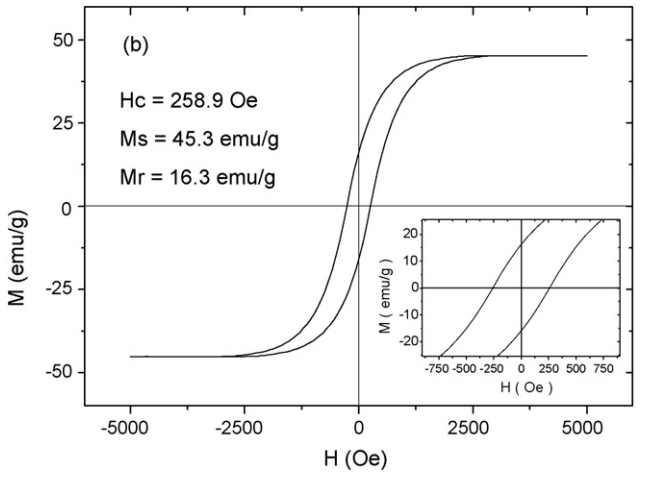

Fig. 8. Hysteresis loops of (a) regular Co-B particles (the inset is the full range of the hysteresis measured between −700 and 700 Oe); (b) mesoporous Co-B particles at room temperature (the inset is the full range of the hysteresis measured between −900 and 900 Oe).

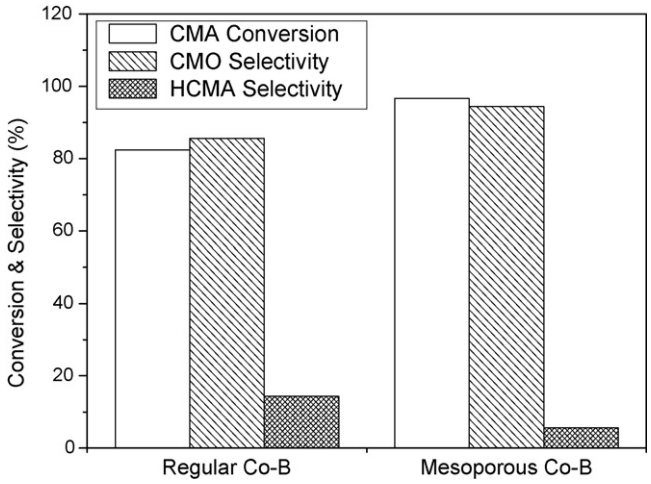

Fig. 10. CMA hydrogenation profile over Co-B particles (a) regular Co-B particles; (b) mesoporous Co-B particles. Reaction conditions: 0.25 g catalyst, 4.5 mL CMA, 40.5 mL ethanol at $PH_2 = 4.2$ MPa and $T = 353$ K for 1.5 h.

From Fig. 10, one can see that the products for the CMA hydrogenation over the as-prepared mesoporous Co-B are dihydrocinnamaldehyde (HCMA) and cinnamyl alcohol (CMO), which are the same as those over regular Co-B. However, the conversion of CMA and the selectivity of CMO over the as-prepared mesoporous Co-B are 96.7% and 94.4%, respectively, which are higher than those of regular Co-B, respectively.

Together with the specific activity data compared in Table 1, one can see that the as-prepared mesoporous Co-B exhibits not only higher catalytic activity but also better selectivity to CMO. The higher activity for the as-prepared mesoporous Co-B is attributed to its larger specific surface area (176.27 m^2/g) (Table 1), which ensures high dispersion of the catalytic active sites [4], and its mesoporous channels, which may facilitate diffusion and adsorption of reactant molecules [12].

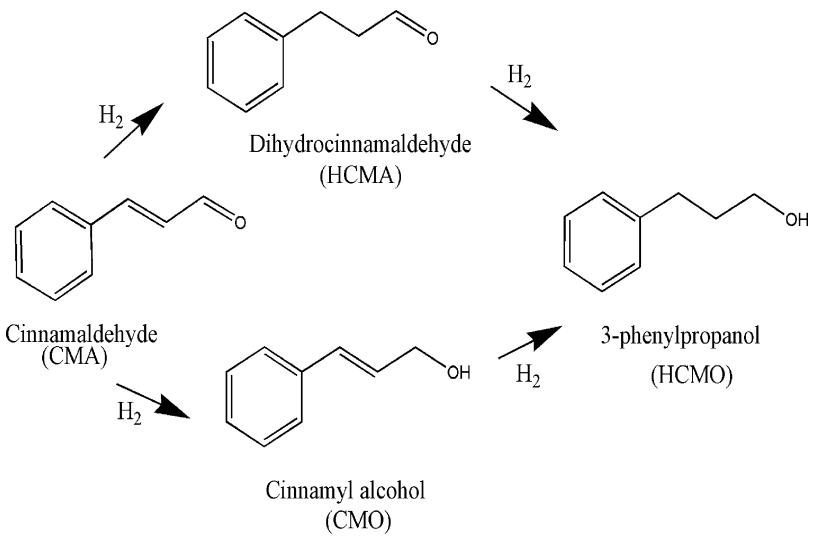

Fig. 9. Reaction scheme for the hydrogenation of CMA.

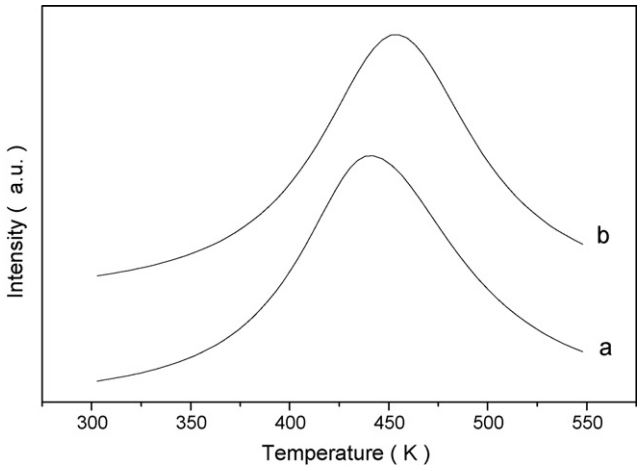

Fig. 11. CO temperature-programmed desorption (TPD) of (a) regular Co-B; (b) mesoporous Co-B.

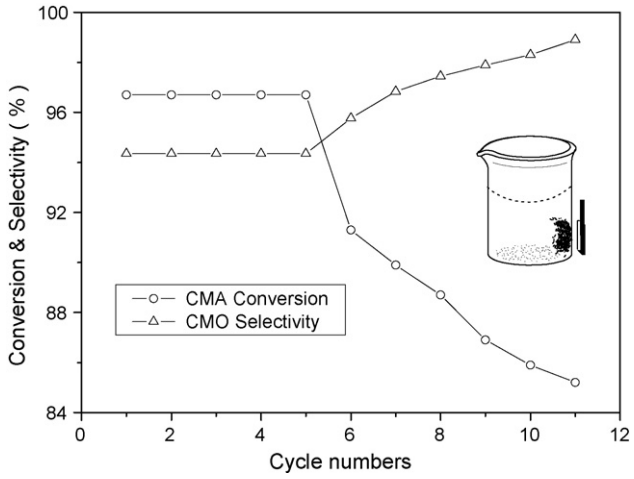

Fig. 13. The conversion of CMA and the selectivity of CMO as functions of cycle numbers over mesoporous Co-B particles. Reaction conditions: 0.25 g catalyst, 4.5 mL CMA, 40.5 mL ethanol at PH_2 = 4.2 MPa and T = 353 K for 1.5 h.

The better selectivity to CMO for the as-prepared mesoporous Co-B might be interpreted by its stronger affinity for C=O bond [1–3], which is shown in the CO temperature-programmed desorption (Fig. 11). Because the stronger adsorption of C=O bond is beneficial to the hydrogenation of CMA via a vertical C=O atop geometry to CMO [3]. The stronger affinity for C=O bond of the as-prepared mesoporous Co-B might be attributed to the relatively more enrichment of B species on the surface compared to the regular Co-B (Table 1). Because the more electrons may transfer from alloying B to the vacant d-orbital of metallic Co for Co-B particles on which surface enriched B [1–3]. As a result, it causes the enhancement of the total adsorption strength of C=O group.

3.6.2. Cycle performance

Fig. 12 presents the typical plot of CMA conversion against CMO selectivity during the CMA hydrogenation over the as-prepared mesoporous Co-B. From Fig. 12, one can see that there is a noticeable trend of increasing selectivity of CMO with increasing conversion of CMA. The optimum yield of CMO (91.3%) was obtained at CMA conversion of 96.7% and CMO selectivity of 94.4%. Further increasing conversion caused an abrupt decrease in the CMO selectivity and thus an abrupt decrease in CMO yield. Therefore, in order to investigate the cycle performance, the reaction condition for the optimum CMO yield was selected for every cycle.

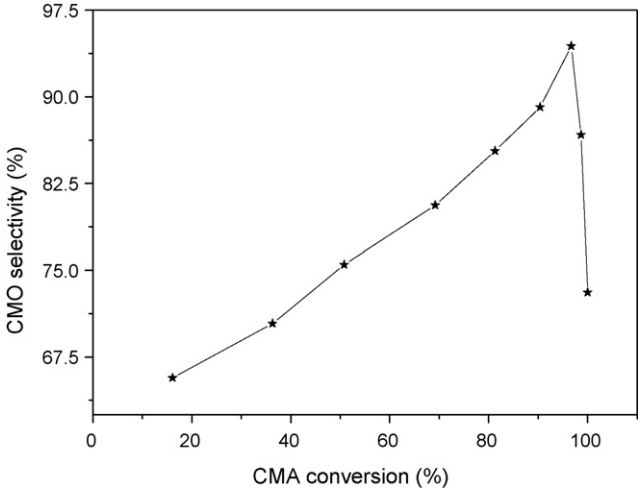

Fig. 12. The typical plot of CMA conversion against CMO selectivity during the CMA hydrogenation over the as-prepared mesoporous Co-B particles. Reaction conditions: 0.25 g catalyst, 4.5 mL CMA, 40.5 mL ethanol at PH_2 = 4.2 MPa and T = 353 K.

Fig. 13 shows the changes of conversion of CMA and selectivity of CMO during cycles for CMA hydrogenation over the as-prepared mesoporous Co-B, respectively. The mesoporous Co-B was recycled by a magnet (the inset of Fig. 13).

From Fig. 13a, one can see that the conversion over five consecutive runs almost remains unchanged, then decreases gradually. The decrease of catalytic activity is attributed to the occurrence of collapse of some mesopores in the cycled mesoporous Co-B, which causes the decrease of specific surface areas during cycling (Table 1). The collapse of some mesopores is revealed by comparison of SEM micrographs of the recycled samples (Fig. 14a and b) after several cycles with the fresh (Fig. 4b). ICP results show that Co leaching during cycling was negligible (Table 1). XPS analyses reveal no occurrences of oxidation for both Co and B on the surface of mesoporous Co-B during cycling (Table 1). The occurrence of collapse for some mesopores during cycling is also confirmed by the constriction of N_2 adsorption–desorption isotherm (Fig. 15), the decreases of pore size and pore volume for the mesoporous Co-B after several cycles (Table 1) [12].

In spite of the existence of collapse of some mesopores, one can see that the conversion of CMA over the mesoporous Co-B after 11 cycles is 85.2% (Fig. 13a), which is higher than that of the fresh regular Co-B (82.4%) (Fig. 10). The higher catalytic activity is attributed to its larger specific surface areas (93.69 m^2/g) (Table 1), which resulted from its preserved mesoporous structure despite the occurrence of collapse of some mesopores, in comparison with the fresh regular Co-B

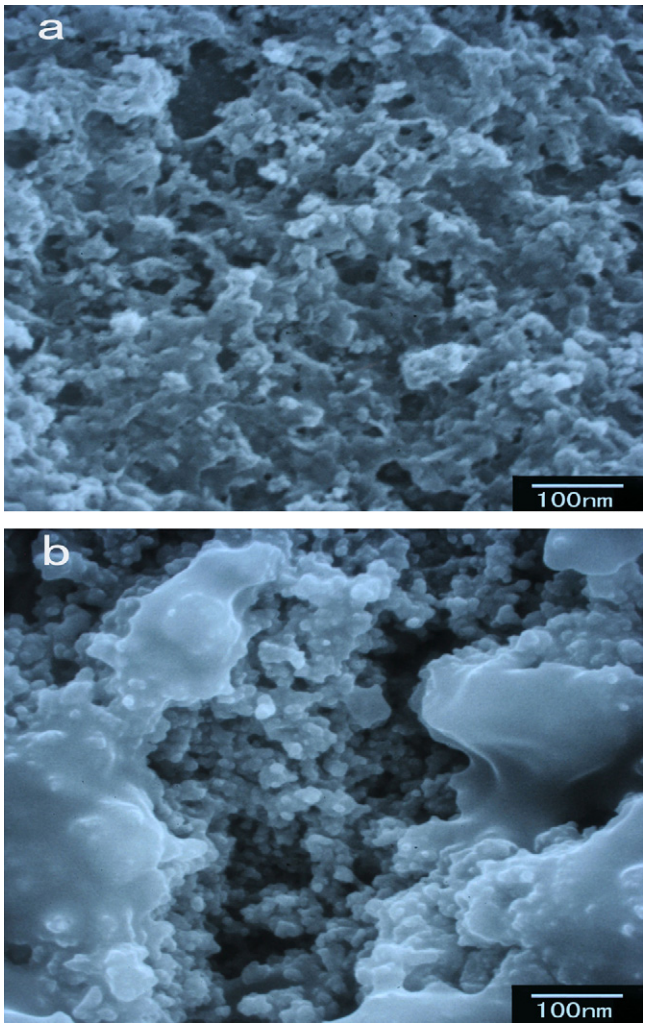

Fig. 14. SEM images of the as-prepared mesoporous Co-B after (a) 6 cycles; (b) 11 cycles.

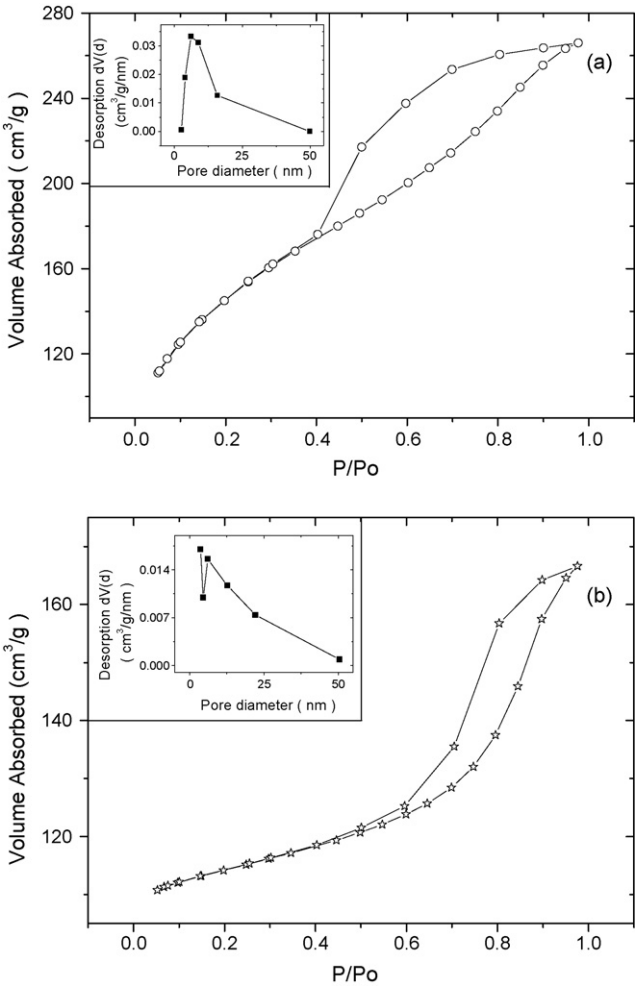

Fig. 15. Nitrogen adsorption–desorption isotherm patterns and the pore size distribution (inset) of mesoporous Co-B after (a) 6 cycles; (b) 11 cycles.

(65.00 m^2/g) (Table 1). The preserved mesoporous structure is revealed by the N_2 adsorption–desorption isotherm of the cycled Co-B that still shows a typical IUPAC type IV pattern (Fig. 15b) [12]. It is also confirmed by that the small-angle XRD patterns of the cycled Co-B, as shown in Fig. 16, still display a well-resolved diffraction peak around of $2\theta = 1.52^\circ$, implying the presence of mesoporous structure in the cycled Co-B. The weak intensity of the diffraction peaks indicates the poor ordering of the mesoporous structure in the as-prepared mesoporous Co-B after several cycles [12].

In addition, in comparison with the typical trend of CMA conversion against CMO selectivity during the CMA hydrogenation over the as-prepared mesoporous Co-B (Fig. 12), the increase of selectivity for CMO after five cycles indicates that the growth of particle size is benefit to the hydrogenation to C=O in CMA [3,18]. The fact of grain growth for amorphous Co-B is observed by comparison of SEM micrographs of the recycled samples (Fig. 14a and b) after several cycles with the fresh (Fig. 4b). The average particle sizes of amorphous Co-B after six cycles and 11 cycles are 60 and 85 nm, respectively. The evaluation for internal diffusion also suggested that the effect of internal diffusion in this work is not distinct in spite of the grain growth for mesoporous Co-B during cycling.

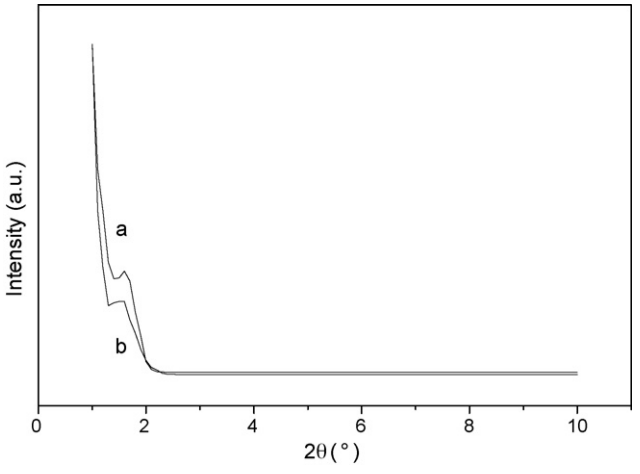

Fig. 16. Small-angle XRD patterns of the as-prepared mesoporous Co-B after (a) 6 cycles; (b) 11 cycles.

4. Conclusions

Amorphous Co-B alloy catalyst with mesoporous structure was firstly prepared via reduction of cobalt acetate by potassium borohydride in the presence of an organic template hexadecyl–trimethyl–ammonium bromide. Investigations demonstrated that such mesoporous structure has a pronounced influence on the magnetic properties of Co-B alloy and the enhanced magnetic performance enables the as-prepared mesoporous Co-B to be recycled by magnetic method in the liquid-phase cinnamaldehyde hydrogenation. During the cinnamaldehyde hydrogenation, the conversion of CMA and the selectivity of CMO over the as-prepared mesoporous Co-B are 96.7% and 94.4%, which are higher than those of regular Co-B, respectively. It is attributed to its larger specific surface area and the stronger affinity to C=O. After 11 cycles, the conversion of cinnamaldehyde over the mesoporous Co-B is 85.2%, which is higher than that of the fresh regular Co-B. The good catalytic activity is attributed to its larger specific surface area resulted from the remaining mesoporous structure in spite of the collapse of some mesopores during cycling. In addition, the increase of selectivity for cinnamyl alcohol during cycling is attributed to the growth of particle size, which is benefit to the hydrogenation to C=O in cinnamaldehyde.

Acknowledgements

This work was supported by the Postdoctoral Foundation of Sichuan Province (0030707602001), the National Natural Sciences Foundation of China (205903603), and 973 project of MST of China (2005CB221400). The authors thank Prof. DAI Xiaoyan and LUO Shizhong for useful discussions.

References

[1] H.X. Li, X.F. Chen, M.H. Wang, Y.P. Xu, Appl. Catal. A: Gen. 225 (2002) 117.
[2] X.F. Chen, H.X. Li, H.S. Luo, M.H. Qiao, Appl. Catal. A: Gen. 233 (2002) 13.
[3] D.G. Tong, W. Chu, Y.Y. Luo, X.Y. Ji, Y. He, J. Mol. Catal. A: Chem. 265 (2006) 196.
[4] J.K. Zeng, J.G. Wang, L.Y. Bi, R.S. Li, Q.B. Kan, Catalytic Action Basis, third ed., Science Press, Beijing, 2005.
[5] G.S. Attard, S.A.A. Leclerc, S. Maniguet, A.E. Russell, I. Nandhakumar, B.R. Gollas, P.N. Bartlett, Microporous Mesoporous Mater. 44–45 (2001) 159.
[6] G.S. Attard, S.A.A. Leclerc, S. Maniguet, A.E. Russell, I. Nandhakumar, P.N. Bartlett, Chem. Mater. 13 (2001) 1444.
[7] H.X. Li, Q.F. Zhao, Y. Wan, W.L. Dai, M.H. Qiao, J. Catal. 244 (2006) 251.
[8] Reference Manual for Operator for PHI PC Windows Software Version 1.2b, Physical Electronic Division, Perkin-Elmer.
[9] B.K. Guo, X.H. Li, S.Q. Yang, Chemical Power Sources, Central South University Press, Changsha, 2002, p. 128.
[10] X.Y. Jin, S.L. Chen, E.N. Yao, Application Guide of Infrared Spectra, Science and Technology Press of Tian Jin, Tian Jin, 1992.
[11] R.A. Nyquist, R.O. Kagel, Infrared Spectra of Inorganic Compounds (3800–45 cm^{-1}), Academic press, New York, 1971.
[12] R.E. Xu, W.Q. Pang, J.H. Yu, Q.S. Hu, J.S. Chen, Chemistry of Molecular Sieve and Porous Materials, Science Press, Beijing, 2004.
[13] A.J. Bard, R. Parsons, J. Jordan, Standard Potentials in Aqueous Solution, Marcel Dekker, New York, 1952, p. 798.
[14] M. Poubaix, Atlas d'Equilibres Electrohimiques, Gauthier-villars, 1963, p. 315.
[15] P. Haasen, R.I. Jatte, Amorphous Metals and Semiconductors, Pergamon, London, 1986.
[16] N.F. Motte, E.A. Davis, Electronic Processes in Non-Crystalline Materials, Clarendon Press, Oxford, 1979.
[17] X.H. Guo, Kinetics for Applied Chemical Engineering, Chemistry Industry Publishing House, Beijing, 2003.
[18] A.G. Fendler, D. Richard, P. Gglezot, Catal. Lett. 5 (1990) 175.